Capacity-Demand-Diagram Methods Based on Inelastic Design Spectrum

Anil K. Chopra, M.EERI, and Rakesh K. Goel, M.EERI

An improved capacity-demand-diagram method that uses the well-known constant-ductility design spectrum for the demand diagram is developed and illustrated by examples. This method estimates the deformation of inelastic SDF systems consistent with the selected inelastic design spectrum, while retaining the attraction of graphical implementation of the ATC-40 *Nonlinear Static Procedure*. One version of the improved method is graphically similar to ATC-40 Procedure A whereas the second version is graphically similar to ATC-40 Procedure B. However, the improved procedures differ from ATC-40 procedures in one important sense. The demand diagram used is different: the constant-ductility demand diagram for inelastic systems in the improved procedure versus the elastic demand diagram in ATC-40 for equivalent linear systems. The improved method can be conveniently implemented numerically if its graphical features are not important to the user. Such a procedure, based on equations relating the yield strength reduction factor, R_y, and ductility factor, μ, for different period, T_n, ranges, has been presented, and illustrated by examples using three different $R_y - \mu - T_n$ relations.

INTRODUCTION

Simplified analysis procedures are presented in the ATC-40 and FEMA-274 documents (Applied Technology Council, 1996; FEMA, 1997) to determine the displacement demand imposed on a building expected to deform inelastically. The *Nonlinear Static Procedure* (NSP) in these documents is based on the Capacity Spectrum Method (CSM) originally developed by Freeman et al. (1975) and Freeman (1978). It consists of the following steps:

1. Develop the relationship between base shear, V_b, and roof (Nth floor) displacement, u_N (Figure 1a), commonly known as the push over curve.
2. Convert the push over curve to a capacity diagram, (Figure 1b), where

$$\Gamma_1 = \frac{\sum_{j=1}^{N} m_j \phi_{j1}}{\sum_{j=1}^{N} m_j \phi_{j1}^2} \qquad M_1^* = \frac{\left(\sum_{j=1}^{N} m_j \phi_{j1}\right)^2}{\sum_{j=1}^{N} m_j \phi_{j1}^2} \tag{1}$$

(AKC) Johnson Professor, Department of Civil & Environmental Engineering, University of California, Berkeley, CA 94720
(RKG) Associate Professor, Department of Civil & Environmental Engineering, California Polytechnic State University, San Luis Obispo, CA 93401

©*Earthquake Spectra*, Volume 15, No. 4, November 1999

and m_j = lumped mass at the jth floor level, ϕ_{j1} is the jth-floor element of the fundamental mode ϕ_1, N is the number of floors, and M_1^* is the effective modal mass for the fundamental vibration mode.

3. Convert the elastic response (or design) spectrum from the standard pseudo-acceleration, A, versus natural period, T_n, format to the $A-D$ format, where D is the deformation spectrum ordinate, to obtain the demand diagram (Figure 1c).
4. Plot the demand diagram and capacity diagram together and determine the displacement demand (Figure 1d). Involved in this step are dynamic analyses of a sequence of equivalent linear systems with successively updated values of the natural vibration period, T_{eq}, and equivalent viscous damping, ξ_{eq}.
5. Convert the displacement demand determined in Step 4 to global (roof) displacement and individual component deformation and compare them to the limiting values for the specified performance goals.

Approximations are implicit in the various steps of this simplified analysis of an inelastic MDF system. Implicit in Steps 1 and 2 is a lateral force distribution assumed to be fixed, and based only on the fundamental vibration mode of the elastic system; however, extensions to account for higher mode effects have been proposed (Paret et al., 1996; Bracci et al., 1997; Gupta and Kunnath, 1999). Implicit in Step 4 is the belief that the earthquake-induced deformation of an inelastic SDF system can be estimated satisfactorily by an iterative method requiring analysis of a sequence of equivalent linear SDF systems with added equivalent viscous damping to account for energy dissipated in yielding, thus avoiding the dynamic analysis of the inelastic SDF system.

The principal objective of this investigation is to develop improved simplified analysis procedures, based on capacity and demand diagrams, to estimate the peak deformation of inelastic SDF systems. The need for such procedures is motivated by first evaluating the above mentioned approximation inherent in Step 4 of the ATC-40 procedure. This brief presentation is based on a comprehensive evaluation of the *Nonlinear Static Procedure* presented in Chopra and Goel (1999, 2000). Thereafter, improved procedures using the well-established inelastic response (or design) spectrum (e.g., Chopra, 1995; Section 7.10) are developed. The idea of using the inelastic design spectrum in this context was suggested by Bertero (1995), and introduced by Reinhorn (1997) and Fajfar (1999); and the capacity spectrum method has been evaluated previously, e.g., Tsopelas et al. (1997).

EVALUATION OF NONLINEAR STATIC PROCEDURE (NSP)

The accuracy of the NSP in estimating the peak deformation of bilinear hysteretic system is evaluated first. For this purpose, the excitation is characterized by the elastic design spectrum of Figure 2 which is the median-plus-one-standard-deviation spectrum constructed by the procedures of Newmark and Hall (1982), as described in Chopra (1995; Section 6.9).

The well-established concepts of constructing the inelastic design spectrum from an elastic design spectrum provide a basis for evaluating this approximate procedure to determine the peak deformations of inelastic systems. This spectrum-based procedure was implemented for a wide range of system periods and ductility values. The yield strength of each bilinear hysteretic system analyzed was chosen corresponding to an allowable ductility μ:

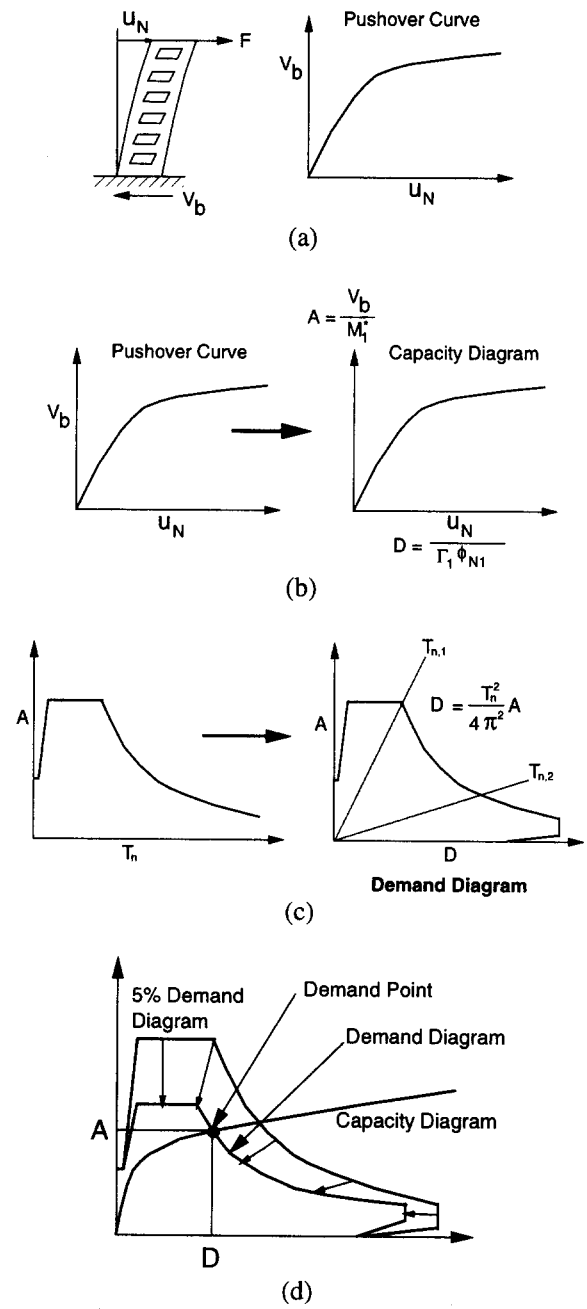

Figure 1. Capacity spectrum method: (a) development of pushover curve, (b) conversion of pushover curve to capacity diagram, (c) conversion of elastic response spectrum from standard format to A-D format, and (d) determination of displacement demand.

$$f_y = (A_y/g)w \tag{2}$$

where w is the weight of the system and A_y is the pseudo-acceleration corresponding to the allowable ductility and the vibration properties – natural period T_n and damping ratio ζ – of the system in its linear range of vibration. Given the properties T_n, ζ, and f_y and the elastic design spectrum, the earthquake induced deformation of the system can be determined as described in Chopra (1995: Section 7.6). Utilized in such a procedure is a T_n-dependent relation between yield strength reduction factor R_y and μ.

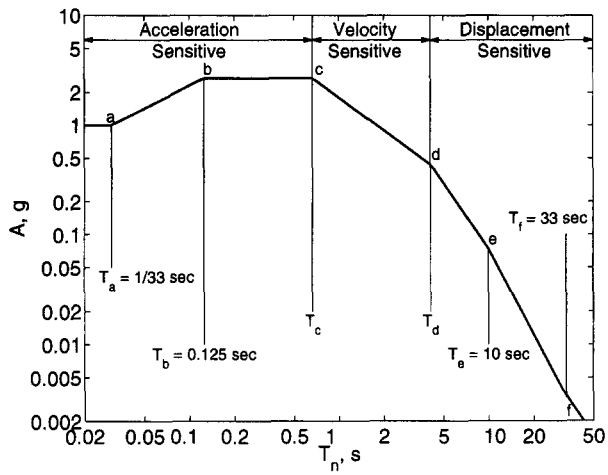

Figure 2. Newmark-Hall elastic design spectrum.

Presented in Figure 3 are the deformations determined by using three different $R_y - \mu - T_n$ equations: Newmark and Hall (1982); Krawinkler and Nassar (1992) for elastoplastic systems; and Vidic, Fajfar and Fischinger (1994) for bilinear systems. The equations describing these relationships are presented later in this paper. Observe that the first two recommendations lead to similar results except for $T_n < 0.3$ sec, indicating that the inelastic design spectrum is a reliable approach to estimate the earthquake-induced deformation of yielding systems, reliable in the sense that different researchers have produced similar results.

The deformation estimates by the ATC-40 method, as determined by Chopra and Goel (1999), are compared in Figure 4 with those in Figure 3 from inelastic design spectra. Relative to these "reference" values, the percentage discrepancy in the approximate result is plotted in Figure 5. The results of Figures 4 and 5 permit the following observations. The approximate procedure leads to significant discrepancy, except for very long periods ($T_n > T_f$ in Figure 2). The magnitude of this discrepancy depends on the design ductility and the period region. In the acceleration-sensitive ($T_n < T_c$) and displacement-sensitive ($T_d < T_n < T_f$) regions (Figure 2), the approximate procedure significantly underestimates the deformation; the discrepancy increases with increasing μ. In the velocity-sensitive ($T_c < T_n < T_d$) region, the ATC-40 procedure significantly underestimates the deformation for $\mu = 2$ and 4, but overestimates it for $\mu = 8$ and is coincidentally accurate for $\mu = 6$.

In passing, note that the ATC-40 procedure is deficient relative to even the *elastic* design spectrum in the velocity-sensitive and displacement-sensitive regions ($T_n > T_c$). For T_n in these regions, the peak deformation of an inelastic system may be taken equal to that of the corresponding elastic system (Veletsos and Newmark, 1960; Chopra, 1995: Section 7.10), and the latter is given by the elastic design spectrum. However, the ATC-40 procedure requires analyses of several equivalent linear systems and still produces worse results.

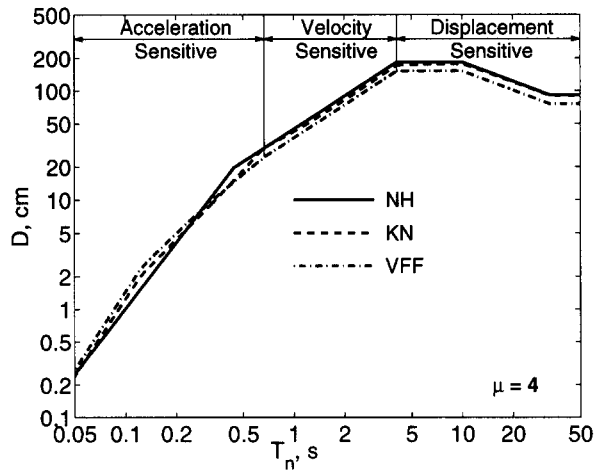

Figure 3. Deformation of inelastic systems (μ= 4) determined from inelastic design spectra using three $R_y - \mu - T_n$ equations: Newmark-Hall (NH), Krawinkler-Nassar (KN), and Vidic-Fajfar-Fischinger (VFF).

IMPROVED PROCEDURES

Presented next are two improved procedures that eliminate the errors (or discrepancies) in the ATC-40 procedures, but retain their graphical appeal. Procedures A and B that are presented are akin to ATC-40 Procedures A and B, respectively. The improved procedures use the well-known constant-ductility design spectrum for the demand diagram, instead of the elastic design spectrum for equivalent linear systems in ATC-40 procedures.

INELASTIC DESIGN SPECTRUM

A constant-ductility spectrum for a bilinear hysteretic system is a plot of A_y versus T_n for selected values of μ. The pseudo-acceleration A_y is related to the yield strength f_y, by Equation 2. The yield strength reduction factor is given by

$$R_y = \frac{f_o}{f_y} = \frac{A}{A_y} \tag{3}$$

where

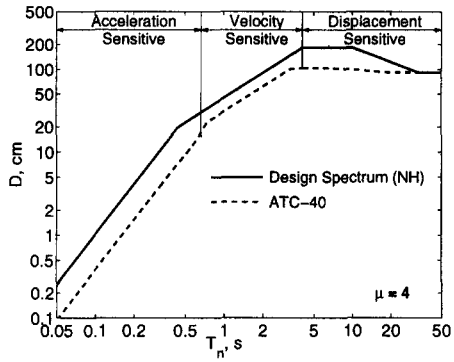

(a)

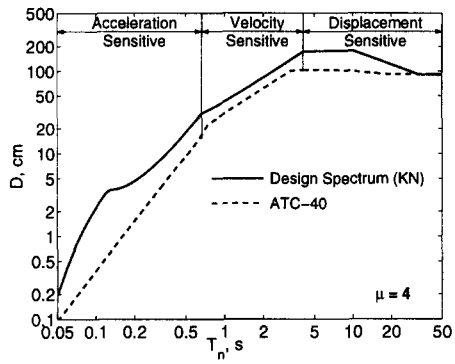

(b)

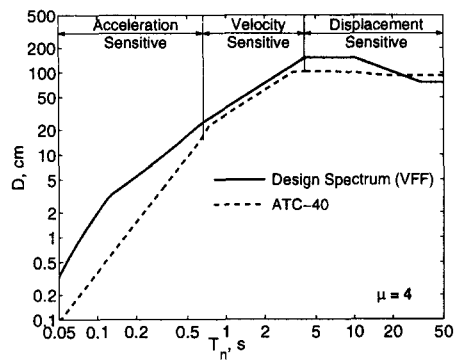

(c)

Figure 4. Comparison of deformations computed by ATC-40 procedure with those from three different inelastic design spectra (μ = 4): (a) Newmark and Hall (1982), (b) Krawinkler and Nassar (1992), and (c) Vidic, Fajfar and Fischinger (1994).

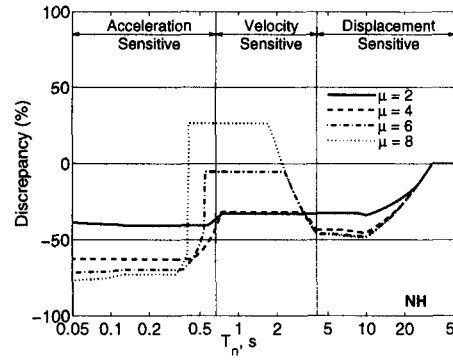

(a)

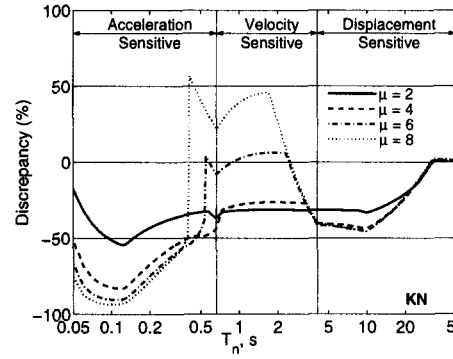

(b)

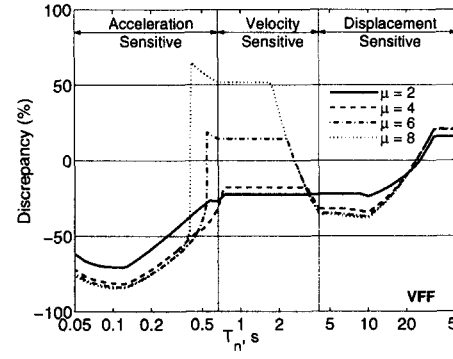

(c)

Figure 5. Discrepancy in deformations computed by ATC-40 procedure relative to three different inelastic design spectra: (a) Newmark and Hall (1982), (b) Krawinkler and Nassar (1992), and (c) Vidic, Fajfar and Fischinger (1994).

$$f_o = \left(\frac{A}{g}\right) w \tag{4}$$

is the minimum yield strength required for the structure to remain elastic during the earthquake; A is the pseudo-acceleration ordinate of the elastic design spectrum at (T_n, ζ).

A constant-ductility design spectrum is established by dividing the elastic design spectrum by appropriate ductility-dependent reduction factors that depend on T_n. The earliest recommendation for the reduction factor, R_y (Equation 3), goes back to the work of Veletsos and Newmark (1960), which is the basis for the inelastic design spectra developed by Newmark and Hall (1982). Starting with the elastic design spectrum of Figure 2 and these $R_y - \mu$ relations for acceleration-, velocity-, and displacement-sensitive spectral regions, the inelastic design spectrum constructed by the procedure described in Chopra (1995, Section 7.10), is shown in Figure 6a.

In recent years, several recommendations for the reduction factor have been developed (Krawinkler and Nassar, 1992; Vidic, Fajfar, and Fischinger, 1994; Riddell, Hidalgo, and Cruz, 1989; Tso and Naumoski, 1991; Miranda and Bertero, 1994). Based on two of these recommendations, the inelastic design spectrum is shown in Figures 6b and 6c. For a fixed μ = 2, the inelastic spectra from Figure 6 are compared in Figure 7. The three spectra are similar in the velocity-sensitive region of the spectrum, but differ in the acceleration-sensitive region.

INELASTIC DEMAND DIAGRAM

The inelastic design spectra of Figure 6 will be plotted in the A-D format to obtain the corresponding demand diagrams. The peak deformation D of the inelastic system is determined as follows:

$$D = \mu D_y \tag{5}$$

with the yield deformation defined by

$$D_y = \left(\frac{T_n}{2\pi}\right)^2 A_y \tag{6}$$

Putting Equations 5 and 6 together gives

$$D = \mu \left(\frac{T_n}{2\pi}\right)^2 A_y \tag{7}$$

Alternatively, by utilizing Equation 3, D can be expressed in terms of the elastic design spectrum

$$D = \mu \frac{1}{R_y} \left(\frac{T_n}{2\pi}\right)^2 A \tag{8}$$

Using Equation 8, D is determined corresponding to the three inelastic design spectra in Figure 7. Such data pairs (A_y, D) are plotted to obtain the demand diagram for inelastic systems (Figure 8).

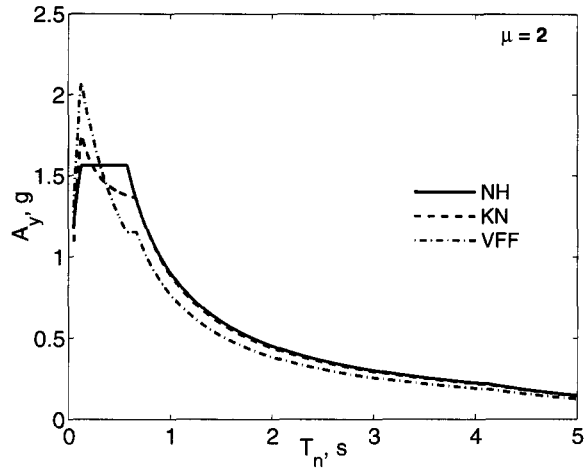

Figure 7. Pseudo-acceleration design spectrum for inelastic systems (μ= 2) using three $R_y - \mu - T_n$ equations: Newmark-Hall (NH), Krawinkler-Nassar (KN), and Vidic-Fajfar-Fischinger (VFF).

PROCEDURE A

This procedure, which uses the demand diagram for inelastic systems (Figure 8), will be illustrated with reference to six elastoplastic systems defined by two values of T_n = 0.5 and 1.0 sec and three different yield strengths, given by Equation 2 using the Newmark-Hall design spectrum (Figure 6a) corresponding to μ = 2, 4, and 6, respectively. For systems with T_n = 0.5 sec, $f_y \div w$ = 1.56, 0.90, and 0.60 for μ = 2, 4, and 6, respectively. The corresponding values for systems with T_n = 1 sec are $f_y \div w$ = 0.90, 0.45, and 0.30. Superimposed on the demand diagrams are the capacity diagrams for three inelastic systems with T_n = 0.5 sec (Figures 9a, 10a, and 11a) and T_n = 1.0 sec (Figures 9b, 10b, and 11b). The yielding branch of the capacity diagram intersects the demand diagram for several μ values. One of these intersection points, which remains to be determined, will provide the deformation demand. At the one relevant intersection point, the ductility factor calculated from the capacity diagram should match the ductility value associated with the intersecting demand curve. Determined according to this criterion, the deformation for each system is noted in Figure 9. This result will be essentially identical to that given by Equation 7. Implementation of this procedure is illustrated next for two systems.

Observe that the estimated deformation is the same for all three systems shown in Figure 9b; T_n = 1 sec for all of them but their yield strengths differ. This result is consistent with the well known "equal displacement rule" (Veletsos and Newmark, 1960; Chopra, 1995: Section 7.10), which says that the deformation of a yielding system with T_n in the velocity- or displacement-sensitive region of the design spectrum is independent of its yield strength and equal to the deformation of the elastic system with the same T_n.

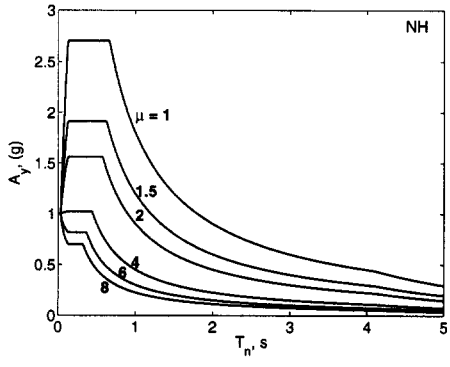

(a)

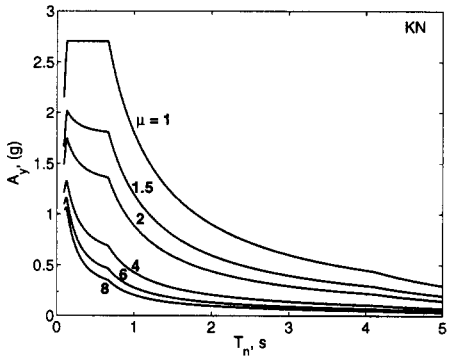

(b)

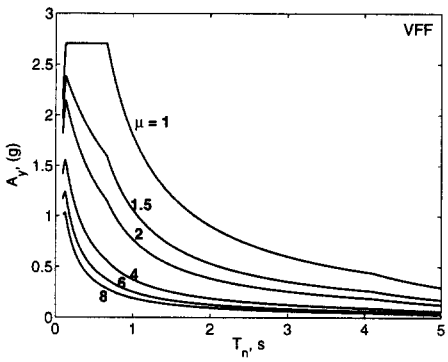

(c)

Figure 6. Inelastic design spectra: (a) Newmark and Hall (1982), (b) Krawinkler and Nassar (1992), and (c) Vidic, Fajfar and Fischinger (1994).

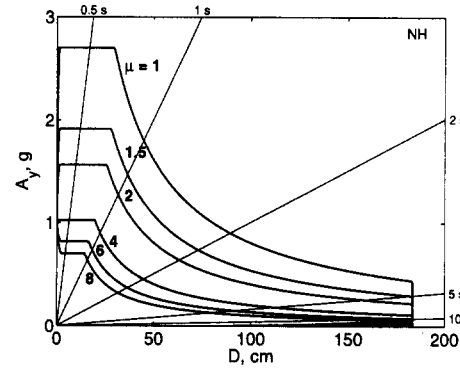

(a)

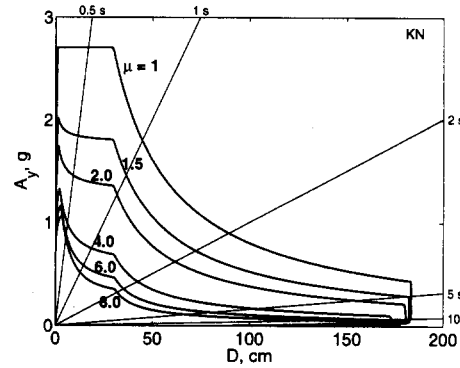

(b)

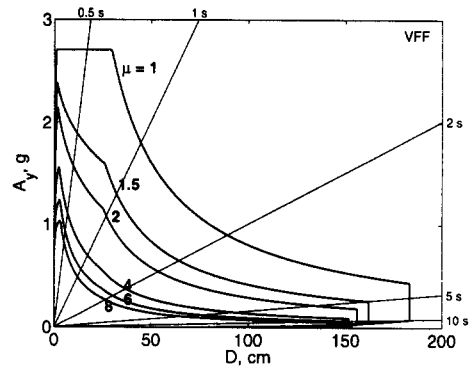

(c)

Figure 8. Inelastic demand diagrams: (a) Newmark and Hall (1982), (b) Krawinkler and Nassar (1992), and (c) Vidic, Fajfar and Fischinger (1994).

Examples

The yield deformation of System 1 (Table 1) is u_y= 3.72cm. The yielding branch of the capacity diagram intersects the demand curves for μ = 1, 2, 4, 6, and 8 at 133.93 cm, 66.96 cm, 33.48 cm, 22.3 cm, and 16.5 cm, respectively (Figure 9a). Dividing by u_y, the corresponding ductility factors are: 133.93÷3.72=35.96 (which exceeds μ = 1 for this demand curve), 66.96÷3.724=17.98 (which exceeds μ = 2 for this demand curve), 33.48÷3.72=8.99 (which exceeds μ = 4 for this demand curve), 22.3÷3.72=6 (which matches μ = 6 for this demand curve), and 16.5÷3.72=4.43 (which is smaller than μ = 8 for this demand curve). Thus, the ductility demand is 6 and the deformation of System 1 is D = 22.3 cm.

For System 3 (Table 1), u_y= 9.68cm. The yielding branch of the capacity diagram intersects the demand curve for μ = 1 at 51.34 cm (Figure 9a). The corresponding ductility factor is 51.34÷9.68=5.3, which is larger than the μ = 1 for this demand curve. The yielding branch of the capacity diagram also intersects the demand curve for μ = 2 continuously from 9.68 cm to 25.2 cm, which correspond to ductility factors of 1 to 2.6. The intersection point at 19.39 cm corresponds to ductility factor = 19.39÷9.68=2 which matches μ = 2 for this demand curve. Thus, the ductility demand is 2 and the deformation of System 3 is D = 19.39 cm.

Observe that for the presented examples, the ductility factor at the intersection point matched exactly the ductility value associated with one of the demand curves because the f_y values were chosen consistent with the same μ values for which the demand curves have been plotted. In general this is not the case and interpolation between demand curves for two μ values would be necessary. Alternatively, the demand curves may be plotted at a finer μ interval avoiding the need for interpolation.

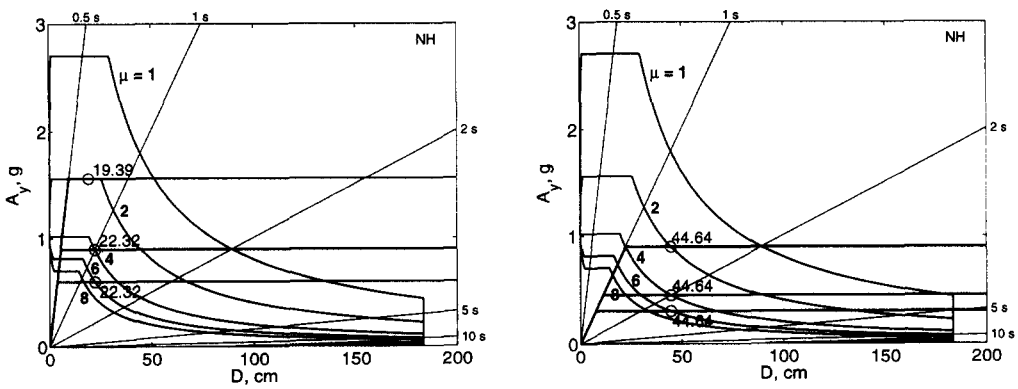

(a) (b)

Figure 9. Application of improved Procedure A using Newmark-Hall (1982) inelastic design spectrum: (a) Systems 1 to 3, and (b) Systems 4 to 6.

This approach was used for analysis of the selected systems using the other two demand diagrams (Figures 8b and 8c). Not all the demand curves at a very fine μ-interval are included, however, in Figures 10 and 11. Only those corresponding to the final values of ductility demand determined by the improved procedure are presented. For example, the ductility demands calculated for system 1 are 5.14 and 4.69 using the Krawinkler-Nassar and Vidic et al. demand diagrams, respectively; demand curves for these μ values are shown in Figures 10a and 11a. These μ values are different than the ductility demand of 6 from the Newmark-Hall demand diagram.

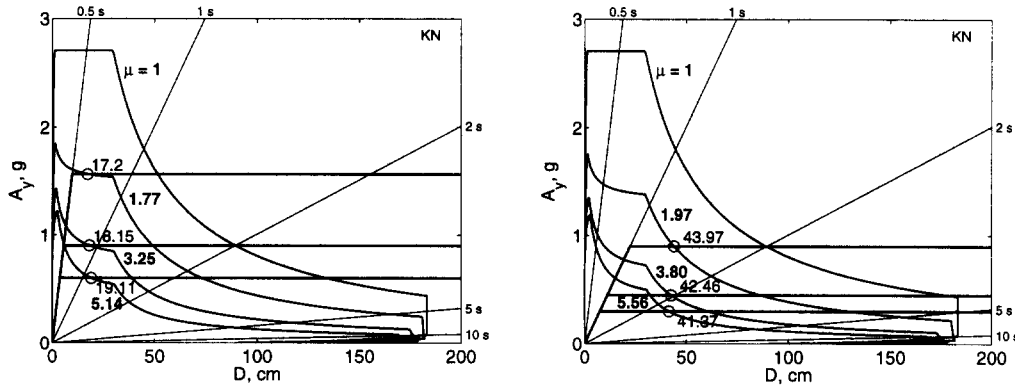

Figure 10. Application of improved Procedure A using Krawinkler-Nassar (1992) inelastic design spectrum: (a) Systems 1 to 3, and (b) Systems 4 to 6.

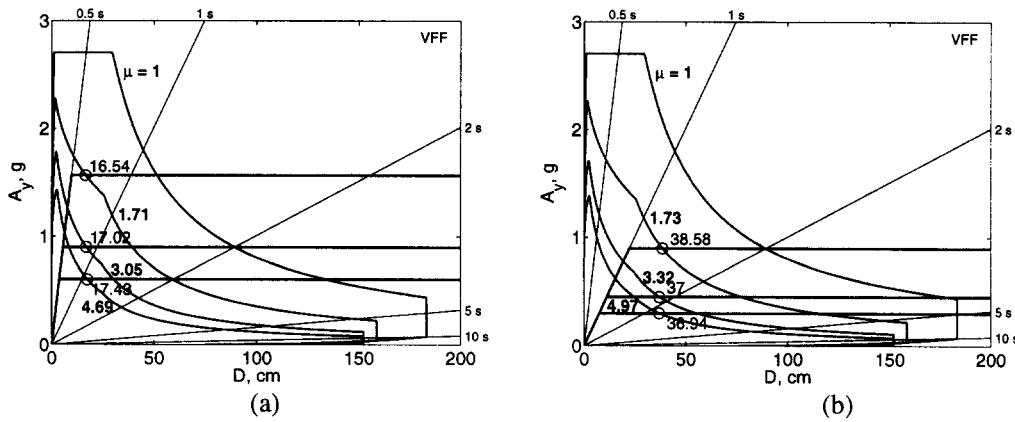

Figure 11. Application of improved Procedure A using Vidic-Fajfar-Fischinger (1994) inelastic design spectrum: (a) Systems 1 to 3, and (b) Systems 4 to 6.

Comparison with ATC-40 Procedure A

The improved procedure just presented gives the deformation value consistent with the selected inelastic design spectrum, while retaining the attraction of graphical implementation of the ATC-40 Procedure A. The two procedures are similar in the sense that the desired

deformation is determined at the intersection of the capacity diagram and the demand diagram. However, the two procedures differ fundamentally in an important sense; the demand diagram used is different: the constant-ductility demand diagram for inelastic systems in the improved procedure (Figures 9 to 11) versus the elastic demand diagram in ATC-40 Procedure A for equivalent linear systems.

PROCEDURE B

This version of the improved procedure avoids construction of the inelastic design spectrum. The peak deformation D of an inelastic system with properties T_n, ζ, and f_y is determined by the following sequence of steps:

1. Plot the capacity diagram and the 5%-damped elastic demand diagram of Figure 2 in A-D format.
2. Assume the expected ductility demand μ; start with $\mu = 1$.
3. Determine $A_y(T_n, \zeta, \mu)$ from the inelastic design spectrum for the estimated μ and calculate D from Equation 7.
4. Plot the point with coordinates D and A_y.
5. Check if the curve generated by connecting similar points intersects the capacity diagram. If not, repeat Steps 3 and 4 with larger values of μ; otherwise go to Step 6.
6. The earthquake-induced deformation demand D is given by the D-value at the intersection point.

Examples

This procedure is implemented for the six systems defined earlier with the earthquake excitation characterized by the elastic design spectrum of Figure 2. The inelastic design spectrum of Newmark and Hall (1982) provides the D_y, A_y pairs for $T_n = 0.5$ sec and 1.0 sec and D is determined by Step 3. The (D, A_y) pairs are plotted to obtain the curve A-B in Figures 12a and 12b. The 5%-damped elastic demand diagram and capacity diagrams for the selected systems are also shown; however, a plot of the elastic demand diagram is not essential to the procedure. The intersection point between the curve A-B and the capacity diagram gives the system deformation: $D = 22.32$ cm, $D = 22.32$ cm and $D = 19.39$ cm for Systems 1, 2, and 3, respectively (Figure 12a) and $D = 44.64$ cm for Systems 4 to 6 (Figure 12b), values same as given by Procedure A. In the latter case, the deformation of the inelastic system is independent of the yield strength and equals that of the corresponding linear system because T_n is in the velocity-sensitive spectral region. This is the well-known equal displacement rule.

Comparison with ATC-40 Procedure B

The improved procedure just presented gives the deformation value consistent with the inelastic design spectrum, while retaining the attraction of a graphical implementation of ATC-40-Procedure B. The two procedures are graphically similar. However, they differ fundamentally in one important sense. Each point on the curve A-B (Figure 12) in the improved procedure is determined by analyzing an inelastic system. In contrast the ATC-40-Procedure B gives a point on the curve A-B by analyzing an equivalent linear system.

ALTERNATIVE DEFINITION OF EQUIVALENT DAMPING

We digress briefly to observe that the capacity spectrum method based on the elastic design spectrum has been modified to use an alternative definition of equivalent viscous damping, ζ_{eq} (Freeman, 1998; WJE, 1996). This ζ_{eq} is derived by equating the peak deformation of the equivalent linear system, determined from the elastic design spectrum (Chopra, 1995; Section 6.9), to the peak deformation of the yielding system, determined from the inelastic design spectrum (Chopra, 1995; Section 7.10). The capacity spectrum method, modified in this way, should give essentially the same deformation as the improved procedure just described. However, we see little benefit in making this detour when the well-known constant-ductility inelastic design spectra can be used directly in the improved procedure.

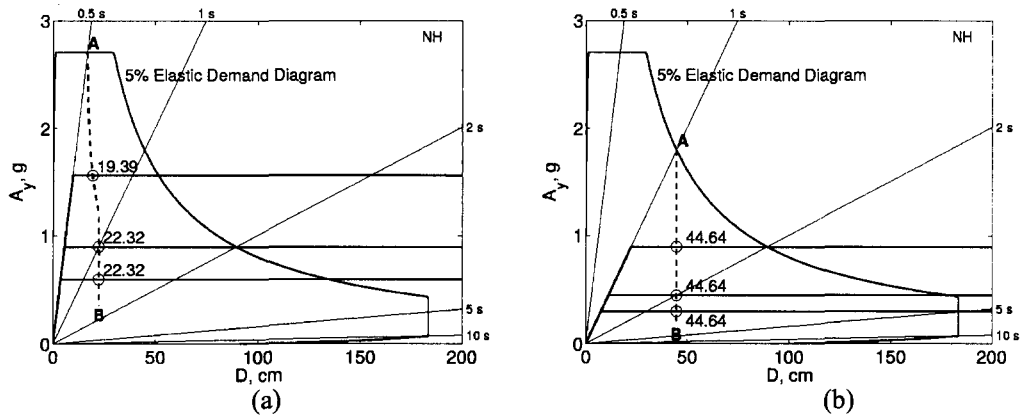

Figure 12. Application of improved Procedure B using Newmark-Hall (1982) inelastic design spectrum: (a) Systems 1 to 3, and (b) Systems 4 to 6.

IMPROVED PROCEDURE: NUMERICAL VERSION

BASIC CONCEPT

The improved procedures presented in the preceding section were implemented graphically, in part, to highlight the similarities and differences relative to the *Nonlinear Static Procedure* in the ATC-40 report. Graphical implementation of Procedure A, the A-version of the improved procedure, is especially attractive as the desired earthquake-induced deformation is determined at the intersection of the capacity and demand diagrams. However, this graphical feature is not essential and the procedure can be implemented numerically. Such a procedure using $R_y - \mu - T_n$ equations is presented in this section.

$R_y - \mu - T_n$ EQUATIONS

The $R_y - \mu - T_n$ equations for elastoplastic systems, consistent with the Newmark-Hall inelastic design spectra are (Chopra, 1995; Section 7.10):

$$R_y = \begin{cases} 1 & T_n < T_a \\ (2\mu - 1)^{\beta/2} & T_a < T_n < T_b \\ \sqrt{2\mu - 1} & T_b < T_n < T_{c'} \\ \dfrac{T_n}{T_c}\mu & T_{c'} < T_n < T_c \\ \mu & T_n > T_c \end{cases} \tag{9a}$$

where

$$\beta = \ln(T_n/T_a)/\ln(T_b/T_a) \tag{9b}$$

and the T_a, T_b, and T_c are defined in Figure 2 and $T_{c'}$ is the period where the constant-A and constant-V branches of the inelastic design spectrum intersect (Chopra, 1995, Section 7.10). Recasting Equation 9 gives μ as a function of R_y:

$$\mu = \begin{cases} \text{Undefined} & T_n < T_a \\ (1 + R_y^{2/\beta})/2 & T_a < T_n < T_b \\ (1 + R_y^2)/2 & T_b < T_n < T_{c'} \\ \dfrac{T_c}{T_n} R_y & T_{c'} < T_n < T_c \\ R_y & T_n > T_c \end{cases} \tag{10}$$

For a given R_y, μ can be calculated for all T_n except for $T_b < T_n < T_c$, wherein two possibilities need to be checked since $T_{c'}$ itself depends on μ (Chopra and Goel, 1999: Appendix B).

Based on the earthquake response of bilinear systems, Krawinkler and Nassar (1992) have developed the following $R_y - \mu - T_n$ equations:

$$R_y = [c(\mu - 1) + 1]^{1/c} \tag{11}$$

where

$$c(T_n, \alpha) = \frac{T_n^a}{1 + T_n^a} + \frac{b}{T_n} \tag{12}$$

and the numerical coefficients depend on the slope αk of the yielding branch: $a = 1$ and $b = 0.42$ for $\alpha = 0\%$; $a = 1$ and $b = 0.37$ for $\alpha = 2\%$; $a = 0.8$ and $b = 0.29$ for $\alpha = 10\%$. Recasting Equation 12 provides μ as a function of R_y:

$$\mu = 1 + \frac{1}{c}(R_y^c - 1) \tag{13}$$

For given values of R_y and α, μ can be calculated from Equation 13.

Based on the earthquake response of bilinear systems, Vidic, Fajfar and Fischinger (1994) have developed the following $R_y - \mu - T_n$ equations:

$$R_y = \begin{cases} 1.35(\mu-1)^{0.95}\dfrac{T_n}{T_o}+1 & T_n \le T_o \\ 1.35(\mu-1)^{0.95}+1 & T_n > T_o \end{cases} \tag{14}$$

where

$$T_o = 0.75\mu^{0.2}T_c \le T_c \tag{15}$$

Recasting Equation 14 gives μ as a function of R_y:

$$\mu = \begin{cases} 1+\left[0.74(R_y-1)\dfrac{T_o}{T_n}\right]^{1.053} & T_n \le T_o \\ 1+\left[0.74(R_y-1)\right]^{1.053} & T_n > T_o \end{cases} \tag{16}$$

Since T_o in Equation 16 depends on μ (Equation 15), the value of μ corresponding to a given R_y is determined by solving a nonlinear equation iteratively unless the simpler relation, $T_o = T_c$, is assumed.

Figure 13 shows plots of R_y versus T_n for selected values of μ based on Equations 9, 11 for $\alpha = 0$, and 14. In Figure 14, μ is plotted against T_n from Equations 10, 13 for $\alpha = 0$, and 16. Observe the similarity among the three sets of results, indicating consensus among different researchers.

The peak deformation of systems 1 to 6 (Table 1) are determined using $R_y - \mu - T_n$ relations of Equations 10, 13, and 16. Detailed calculations are presented in Chopra and Goel (1999: Appendix B) and the results are summarized in Table 1. Observe that the deformation values computed using $R_y - \mu - T_n$ equations are identical to those determined by the graphical procedure (Figures 9 to 11) except for round-off differences. For comparison, the peak deformation values determined by the ATC-40 procedure have also been included. It is clear that the ATC-40 values are generally too unconservative, compared to the deformation determined from three $R_y - \mu - T_n$ equations (recommended by different researchers), all of which give similar values. The data in Table 1 for six systems is a small subset of the results plotted in Figures 3 and 4.

Table 1. Results from numerical implementation of improved procedure using three $R_y - \mu - T_n$ equations.

System Properties						Newmark-Hall		Krawinkler-Nassar		Vidic et al.		ATC-40
System	T_n (s)	A (g)	A_y ($f_y \div w$) (g)	$D_y = u_y$ (cm)	R_y ($A \div A_y$)	μ (Eq. 16)	D ($\mu \times D_y$) (cm)	μ (Eq. 19)	D ($\mu \times D_y$) (cm)	μ (Eq. 22)	D ($\mu \times D_y$) (cm)	D (cm)
1	0.5	2.71	0.60	3.72	4.51	5.99	22.29	5.14	19.11	4.69	17.43	10.46
2			0.90	5.58	3.01	3.99	22.29	3.25	18.15	3.05	17.02	9.25
3			1.56	9.70	1.73	2.00	19.39	1.77	17.20	1.71	16.54	11.51
4	1	1.80	0.30	7.44	6.00	6.00	44.64	5.56	41.37	4.97	36.94	42.27
5			0.45	11.16	4.00	4.00	44.64	3.80	42.46	3.32	37.00	30.45
6			0.90	22.32	2.00	2.00	44.64	1.97	43.97	1.73	38.58	29.84

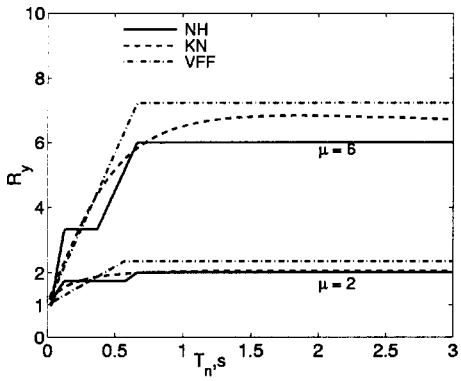

Figure 13. Variation of R_y with T_n for selected ductility values based on three different sources: Newmark and Hall (1982), Krawinkler and Nassar (1992), and Vidic, Fajfar, and Fischinger (1994).

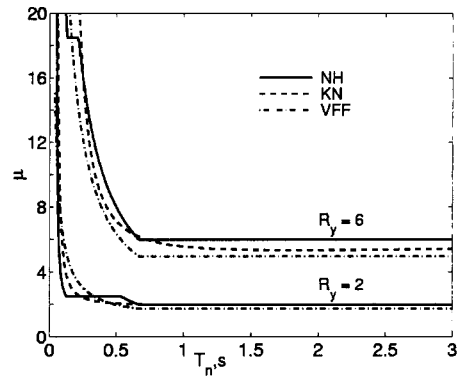

Figure 14. Variation of μ with T_n for selected R_y values based on three different sources: Newmark and Hall (1982), Krawinkler and Nassar (1992), and Vidic, Fajfar, and Fischinger (1994).

CONSISTENT TERMINOLOGY

Many new terms that have been introduced in the ATC-40 report and related publications in connection with simplified analysis of inelastic systems are examined in this section and, where necessary, better (in our opinion) terminology is recommended:

1. *Demand Spectrum.* The term "spectrum" has traditionally implied a function of frequency or period. For example, *response spectrum* is a plot of the peak value of a response quantity as a function of the natural vibration period (or frequency) of an SDF system. Another example: *Fourier Spectrum* of ground acceleration is a plot of the amplitude of the Fourier transform of the excitation against exciting frequency. The "Response Spectrum" terminology was introduced in the 1930s within the context of earthquake engineering, whereas the "Fourier Spectrum" terminology has existed for much longer. Given this background, "spectrum" is inappropriate to describe a plot of pseudo-acceleration versus deformation. The terminology *Demand Diagram* has therefore been used in this paper.
2. *Capacity Spectrum.* For the same reasons, the recommended terminology is *Capacity Diagram.*
3. *Acceleration-Displacement Response Spectrum (ADRS) Format.* For the same reasons, the recommended terminology is *A-D* format.
4. *Modal Participation Factor.* This traditional terminology for Γ_n (Equation 1) implies that it is a measure of the degree to which the nth mode participates in the response. However, this is misleading because Γ_n is not independent of how the mode is normalized, nor a measure of the modal contribution to a response quantity (Chopra, 1995; Section 13.1).

CONCLUSIONS

This investigation of capacity-demand-diagram methods to estimate the earthquake-induced deformation of inelastic SDF systems has led to the following conclusions:

1. The ATC-40 procedures were implemented for a wide range of T_n and μ values with the excitation characterized by an elastic design spectrum. The resulting estimate of deformation for the inelastic system was compared with the deformation determined from the inelastic design spectrum using three different $R_y - \mu - T_n$ equations (Newmark and Hall, 1982; Krawinkler and Nassar, 1992; Vidic, Fajfar, and Fischinger, 1994), all of which provided similar results. Relative to these "reference" values, the approximate procedure significantly underestimates the deformation for a wide range of T_n and μ values.

2. The ATC-40 procedures are deficient relative to even the elastic design spectrum in the velocity- sensitive and displacement-sensitive regions of the spectrum. For T_n in these regions, the peak deformation of an inelastic system can be estimated from the elastic design spectrum using the well-known equal displacement rule. However, the approximate procedure requires analyses of several equivalent linear systems and still produces worse results.

3. An improved capacity-demand-diagram method that uses the well-known constant-ductility design spectrum for the demand diagram has been developed and illustrated by examples. When both capacity and demand diagrams are plotted in the *A-D* format, the yielding branch of the capacity diagram intersects the demand curves for several μ values. The deformation is given by the one intersection point where the ductility factor calculated from the capacity diagram matches the value associated with the intersecting demand curve. This deformation is identical to the value determined by the well-established Equation 7 using the selected inelastic design spectrum, while retaining the attraction of graphical implementation of the ATC-40 methods.

4. One version of the improved method is graphically similar to ATC-40 Procedure A. However, the two differ fundamentally in an important sense; the demand diagram used is different: the constant-ductility demand diagram for inelastic systems in the improved procedure versus the elastic demand diagram in ATC-40 for equivalent linear systems.

5. A second version of the improved method is graphically similar to ATC-40 Procedure B. However the two differ fundamentally in one important sense. Each point on curve A-B is determined by analyzing an inelastic system in the improved procedure (Figure 12) but an equivalent linear system in ATC-40.

6. The improved method can be conveniently implemented numerically if its graphical features are not important to the user. Such a procedure, based on equations relating R_y and μ for different T_n ranges, has been presented and illustrated by examples using three different $R_y - \mu - T_n$ relations (Newmark and Hall, 1982; Krawinkler and Nassar, 1992; Vidic, Fajfar, and Fischinger, 1994). The graphical and numerical implementations of the improved method are shown to give essentially identical values of deformation.

7. The new terminology that has been introduced in the ATC-40 report and related publications in connection with simplified analysis of inelastic systems has been examined and, where necessary, better terminology recommended:

   (a) The term "spectrum" implies a function of frequency or period (e.g., response spectrum or Fourier spectrum) and is therefore inappropriate to describe a plot of

pseudo-acceleration versus deformation. The recommended terminology is *Demand Diagram* and *Capacity Diagram* instead of *Demand Spectrum* and *Capacity Spectrum.*

(b) *Acceleration-Displacement Response Spectrum (ADRS) Format* is inappropriate for the same reason and *A-D Format* is preferable.

In this paper we have focussed on improving the one step in the NSP or CSM to determine the earthquake induced deformation demand of an inelastic SDF system. We have demonstrated here and in Chopra and Goel (2000) that the equivalent linear system approach, as implemented in these methods, generally gives unacceptably unconservative estimates of deformation due to far-field ground motions; it is expected to be even worse for near-field ground motions. Fortunately, this approach is not necessary to achieve a simplified analysis procedure suitable for design of new structures or evaluation of existing structures. In particular, the improved capacity-demand-diagram method presented here, while retaining the simplicity and graphical appeal of the NSP and CSM, provides results consistent with selected elastic design spectrum and chosen rules for constructing the inelastic design spectrum. Although illustrated for elastoplastic systems, this method is extendable to any force-deformation relation. However, additional work is necessary to evaluate approximations inherent in other steps of the NSP and CSM – in computing the pushover curve for a MDF system and converting it to a capacity diagram.

ACKNOWLEDGEMENTS

This research investigation is funded by the National Science Foundation under Grant CMS-9812531, a part of the U.S.-Japan Cooperative Research in Urban Earthquake Disaster Mitigation. This financial support is gratefully acknowledged. The authors have benefited from discussions with Chris D. Poland and Wayne A. Low, who are working on a companion research project awarded to Degenkolb Engineers; and with Sigmund A. Freeman, who, more than any other individual, has been responsible for the concept and development of the capacity spectrum method.

REFERENCES

Applied Technology Council, 1996, *Seismic Evaluation and Retrofit of Concrete Buildings*, Report ATC 40, November.

Bertero, V. V., 1995, Tri-service manual methods, in *Vision 2000*, Part 2, Appendix J, Structural Engineers Association of California, Sacramento.

Bracci, J. M., Kunnath, S. K., and Reinhorn, A. M., 1997, Seismic Performance and Retrofit Evaluation of Reinforced Concrete Structures, *Journal of Structural Engineering*, ASCE, **123**, 3-10.

Chopra, A. K., 1995, *Dynamics of Structures: Theory and Applications to Earthquake Engineering*, Chapters 6, 7, and 13, Prentice Hall, New Jersey.

Chopra, A. K. and Goel, R. K., 1999, *Capacity-Demand-Diagram Methods for Estimating Seismic Deformation of Inelastic Structures: SDF Systems*, Report No. PEER-1999/02, Pacific Earthquake Engineering Research Center, University of California, Berkeley, April.

Chopra, A. K. and Goel, R. K., 2000, Evaluation of a NSP to Estimate Seismic Deformation: SDF System, To Appear, *Journal of Structural Engineering*, ASCE, January.

Fajfar, P., 1999, Capacity Spectrum Method based on Inelastic Spectra, *Earthquake Engineering and Structural Dynamics*, **28**, 979-993.

FEMA, 1997, *NEHRP Guidelines for the Seismic Rehabilitation of Buildings,* FEMA 273; and *NEHRP Commentary on the Guidelines for the Seismic Rehabilitation of Buildings*, FEMA 274, October, Federal Emergency Management Agency, Washington, D.C.

Freeman, S. A., Nicoletti, J. P., and Tyrell, J. V., 1975, Evaluations of existing buildings for seismic risk - A case study of Puget Sound Naval Shipyard, Bremerton, Washington, *Proceedings of 1st U.S. National Conference on Earthquake Engineering*, EERI, Berkeley, 113-122.

Freeman, S. A., 1978, Prediction of response of concrete buildings to severe earthquake motion, *Publication SP-55,* American Concrete Institute, Detroit, MI, 589-605.

Freeman, S. A., 1998, Development and use of capacity spectrum method, *Proceedings of 6th U.S. National Conference on Earthquake Engineering*, Seattle, CD-ROM, EERI, Oakland.

Gupta, B. and Kunnath, S. K., 1999, Adaptive Spectra-Based Pushover Procedure for Seismic Evaluation of Structures, Submitted for Publication to *Earthquake Spectra.*

Krawinkler, H. and Nassar, A. A., 1992, Seismic design based on ductility and cumulative damage demands and capacities, in *Nonlinear Seismic Analysis and Design of Reinforced Concrete Buildings*, P. Fajfar and H. Krawinkler, Eds., Elsevier Applied Science, New York.

Miranda, E. and Bertero, V. V., 1994, Evaluation of strength reduction factors for earthquake-resistant design, *Earthquake Spectra*, **10**, 357-379.

Newmark, N. M. and Hall, W. J., 1982, *Earthquake Spectra and Design.* Earthquake Engineering Research Institute, Berkeley, CA.

Paret, T. F., Sasaki, K. K., Eilbekc, D. H., and Freeman, S. A., 1996, Approximate inelastic procedures to identify failure mechanisms from higher mode effects, Paper No. 966, *11th World Conference on Earthquake Engineering*, Acapulco, Mexico.

Reinhorn, A. M., 1997, Inelastic analysis techniques in seismic evaluations, P. Fajfar and H. Krawinkler (eds.), *Seismic design methodologies for the next generation of codes*, Balkema, Rotterdam, 277-287.

Riddell, R., Hidalgo, P., and Cruz, E., 1989, Response modification factors for earthquake resistant design of short period buildings, *Earthquake Spectra*, **5**, 571-590.

Tso, W. K. and Naumoski, N., 1991, Period-dependent seismic force reduction factors for short-period structures, *Canadian Journal of Civil Engineering*, **18**, 568-574.

Tsopelas, P., Constantinou, M. C., Kircher, C. A., and Whittaker, A. S., 1997, *Evaluation of simplified methods of analysis for yielding structures*, Report No. NCEER-97-0012, State University of New York at Buffalo, N.Y.

Veletsos, A. S. and Newmark, N. M., 1960, Effects of inelastic behavior on the response of simple system to earthquake motions, *Proceedings of the 2nd World Conference on Earthquake Engineering*, Japan, **2**, 895-912.

Vidic, T., Fajfar, P., and Fischinger, M., 1994, Consistent inelastic design spectra: strength and displacement, *Earthquake Engineering and Structural Dynamics*, **23**, 507-521.

WJE, 1996, *Seismic Dynamic Analysis for Buildings*, Final Manuscript prepared for the U.S. Army Engineering Division by Wiss, Janney, Elstner Associates, Inc., Emeryville, CA (Unpublished).

NOTATION

α	strain hardening ratio
a	constant used in Krawinkler and Nassar $R_y - \mu - T_n$ equations
β	constant used in Newmark and Hall $R_y - \mu - T_n$ equations
A	pseudo-acceleration spectrum ordinate
A_y	$(2\pi/T_n)^2 D_y$, pseudo-acceleration corresponding to yield deformation D_y

b	constant used in Krawinkler and Nassar $R_y - \mu - T_n$ equations
c	variable used in Krawinkler and Nassar $R_y - \mu - T_n$ equations
D	deformation spectrum ordinate
D_y	yield deformation = u_y
ϕ_1	fundamental mode
ϕ_{j1}	j^{th} floor element of the fundamental mode ϕ_1
f_o	minimum strength required for a system to remain elastic
f_y	yield strength
g	acceleration due to gravity
k	initial elastic stiffness
Γ_1	fundamental mode factor defined by Equation 1
m	mass of the system
m_j	lumped mass at the jth floor level
M_1^*	effective modal mass for the fundamental vibration mode
N	number of floors
μ	ductility factor
R_y	yield reduction factor
$T_a, T_b, T_c, T_{c'}, T_d, T_e, T_f$	periods that define spectral regions
T_o	transition period used in Vidic, Fajfar, and Fischinger $R_y - \mu - T_n$ equations
T_{eq}	equivalent vibration period
T_n	natural vibration period
u_N	roof displacement
u_y	yield displacement
V_b	base shear
w	weight of the system
ζ	viscous damping ratio of linearly elastic system
ζ_{eq}	viscous damping used in equivalent linear procedures